




Fluid–structure interaction study on the performance of flexible articulated caudal fin

Bo Liu, Shiwu Zhang, Fenghua Qin & Jie Yang


To cite this article: Bo Liu, Shiwu Zhang, Fenghua Qin & Jie Yang (2014) Fluid–structure interaction study on the performance of flexible articulated caudal fin, *Advanced Robotics*, 28:24, 1665-1676, DOI: [10.1080/01691864.2014.957722](https://doi.org/10.1080/01691864.2014.957722)

To link to this article: <http://dx.doi.org/10.1080/01691864.2014.957722>

 View supplementary material [↗](#)


 Published online: 22 Dec 2014.

 Submit your article to this journal [↗](#)

 Article views: 146

 View related articles [↗](#)

 View Crossmark data [↗](#)

 Citing articles: 5 View citing articles [↗](#)

FULL PAPER

Fluid–structure interaction study on the performance of flexible articulated caudal fin

Bo Liu^a, Shiwu Zhang^{a*}, Fenghua Qin^b and Jie Yang^a

^aDepartment of Precision Machinery and Precision Instrumentation, University of Science and Technology of China, Hefei, Anhui 230026, P.R. China; ^bDepartment of Modern Mechanics, University of Science and Technology of China, Hefei, Anhui 230026, P.R. China

(Received 15 April 2014; revised 01 July 2014 accepted 12 August 2014)

In this paper, the propulsive performance of a flexible articulated caudal fin is investigated by fluid–structure interaction. The caudal fin is composed of two links which are connected by a hinge. One link is driven by pitching motion while the other one moves passively. Five cases of link flexibility are investigated, namely, the rigid–rigid case, the medium flexible–medium flexible case, the flexible–flexible case, the rigid–flexible case and the flexible–rigid case. Their fluid field and structure deformations are analysed and hydrodynamic forces are compared. It is found that the rigid–rigid caudal fin produces larger thrust force than other cases with a low-pitching frequency, while the rigid–flexible case performs better with a higher frequency. The mean thrust force increases with the frequency in our experiments, however, for the medium flexible–medium flexible case, an optimal frequency exists. Besides, the effect of the hinge stiffness is studied. It is seen that the medium flexible–medium flexible case exhibits a striking performance. When the hinge stiffness decreases, its mean thrust force increases and possesses larger amplitude while the forces of other cases decrease. These results can guide the design of flexible propeller with links and will be useful for the development of flexible underwater robots.

Keywords: fluid–structure interaction; articulated caudal fin; flexibility; hydrodynamic forces

1. Introduction

Caudal fin propulsion has been an intriguing problem for decades and subjects to a variety of studies including theoretical model, numerical simulation, morphology and kinematic study, fin prototype design and so on.[1–9] Nowadays, more and more interest is focused on its flexible structure's effect on the hydrodynamic force. Since in nature, the fins are flexible, this phenomenon inspires researchers that the flexible structures possess some advantages compared with the rigid ones. Many investigations have been conducted to analyse the performance of the flexible fins, ranging from span-wise flexibility [10,11] to chord-wise flexibility [12,13] or even variable flexibility.[14,15] Meanwhile, the strong coupling of the structure and fluid is simulated by computational schemes.[16–19] For example, Zhu and Shoele numerically investigated the propulsion performance of a skeleton-strengthened caudal fin they computed with two unsteady motions, and studied the fin's deformation and thrust coefficient and propulsion efficiency [18]. Esposito et al. also developed a robotic fish caudal fin with five sets of fin rays which exhibited different stiffness, and they investigated their influence on the generation of thrust force and lift force.[20]

Among these models to analyse the fins/wings flexibility, one interesting endeavour is to simplify the fins/

wings into several links which are connected by hinges/torsion spring.[21–24] One link moves with prescribed motions, while the others rotate passively under the inertial force and hydrodynamic/aerodynamic force. Toomey and Eldredge investigated a two-component structure, and analysed the lift force and hinge deflection.[23] Wan et al. conducted direct numerical simulation on the hinged plates; they varied the location of the hinge and investigated the thrust and lift forces, and an incidence angle limiter was also used to control the lower link angle.[24] However, their simplified models took only the hinge flexibility into consideration, and still use the rigid segments/links as discrete elements for the fins/wings. In fact, for a multi-rigid-links structure, the continuous deformation of the system is transferred to the rotation of articulation, which discretises the flexibility and simplifies the degree of freedom. However, for a more complex case: in a multi-flexible-links structure, which combines continuous deformation and discrete deformation into a propeller, less attention is paid and its hydrodynamic performance still remains unknown.

In the present study, a caudal fin with two links is modelled as the propulsion element of a simplified fish model of which a two-dimensional model is built as shown in Figure 1. The link flexibility and hinge stiffness are considered together to determine the flexibility of the whole caudal fin. The flexibility of the two links

*Corresponding author. Email: swzhang@ustc.edu.cn

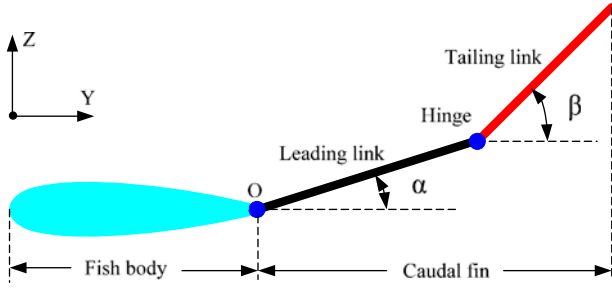


Figure 1. Sketch of the fish model.

varies from rigid to flexible, respectively. Total five groups of the link flexibility are investigated, namely, the rigid–rigid case, the medium flexible–medium flexible case, the flexible–flexible case, the rigid–flexible case and the flexible–rigid case. Their fluid field and structure deformations are analysed, and the thrust and lift forces are compared.

The remainder of the paper is organised as follows. Section 2 introduces the computational models and the numerical method. Section 3 presents the detailed simulation results. Section 4 is the result discussion and Section 5 concludes the paper.

2. Model and numerical method

2.1. Model development

The fish caudal fin is a three-dimensional flexible structure, which possesses chord-wise deformation, spans-wise bending or torsion. In this article, we only account for the chord-wise flexibility and take a section of the three-dimensional fin into consideration which is simple but enough to extract the core dynamics.[12,25,26] Figure 1 shows the sketch of the two-dimensional fish model. It consists of two parts. The first part is a ‘tear drop’ shape which is used to represent the fish body for simplicity. The second part is the caudal fin which is composed of two links, the leading link and the tailing link. The two links are connected by a hinge where a torsion spring is applied to mimic the flexibility among the links.

2.2. Kinematics modelling

The whole fish model is still in the flowing water by fixing the fish body, but the caudal fin can move and deform to generate forces. The leading link performs a prescribed motion around its leading point O which is defined by

$$\alpha = \theta_0 + \theta_a \sin(2\pi ft - \alpha_0) \quad (1)$$

where θ_a stands for the pitching amplitude and θ_0 stands for the initial pitching angle (which is 0 in this paper indicating it starts from the equilibrium position). f stands for the pitching frequency. And α_0 is the initial phase angle which is set as 0 in the article.

The tailing link moves passively. The rotation angle β is unknown and determined by the solid structure and fluid together. The flexibility of the two links is also varied from rigid to flexible which indicates the links themselves will undergo deformations.

2.3. Governing equations

For the fluid domain, the Arbitrary–Lagrangian–Eulerian (ALE) method is used which can solve the deformation of boundaries compared with traditional Eulerian method. The continuity and momentum equations in ALE description are expressed as follows [27,28]:

$$\nabla \cdot \mathbf{v} = 0 \quad (2)$$

$$\rho_f \frac{\rho \mathbf{v}}{\rho t} + \rho_f [(\mathbf{v} - \mathbf{w} \cdot \nabla)] \mathbf{v} = \nabla \cdot \boldsymbol{\tau}_f + \mathbf{f}_f^B \quad (3)$$

where \mathbf{v} stands for the flow velocity vector, and \mathbf{w} stands for the velocity vector of the moving ALE frame; if $\mathbf{w} = 0$, the ALE frame does not move indicating that the Eulerian formulation is used, if $\mathbf{w} = \mathbf{v}$, the ALE frame moves with the fluid particles indicating that the Lagrangian formulation is used. ρ_f is the fluid density, $\boldsymbol{\tau}_f$ is the fluid stress tensor and is shown in Equations (4) and (5). p is the fluid pressure, μ is the viscosity of the fluid, δ_{ij} is the Kronecker delta and ε_{ij} is the strain rate. The body force \mathbf{f}_f^B is neglected for the fluid analysis and gravity force is not considered.

$$\boldsymbol{\tau}_f = -p\delta_{ij} + 2\mu\varepsilon_{ij} \quad (4)$$

$$\varepsilon_{ij} = \frac{1}{2} (\nabla \mathbf{v} + \nabla \mathbf{v}^T) \quad (5)$$

For the structure domain, the Lagrangian method is used to calculate the displacement and force.

$$\rho_s \frac{\partial^2 \mathbf{u}_s}{\partial t^2} = \nabla \cdot \boldsymbol{\tau}_s + \mathbf{f}_s^B \quad (6)$$

where ρ_s is the structure density, \mathbf{f}_s^B is the vector of body force, $\boldsymbol{\tau}_s$ is the structure stress tensor and \mathbf{u}_s is the vector of the structural displacement.

On the coupling interface, another two equations are obtained to solve the kinematics and dynamics equilibrium.

$$\underline{\mathbf{u}}_f = \underline{\mathbf{u}}_s \quad (7)$$

$$\mathbf{n} \cdot \underline{\boldsymbol{\tau}}_f = \mathbf{n} \cdot \underline{\boldsymbol{\tau}}_s \quad (8)$$

The \underline{u}_f and \underline{u}_s stand for the displacement of the fluid and structure on the coupling interface, respectively, the $\underline{\tau}_f$ and $\underline{\tau}_s$ stand for the stress of the fluid and structure, respectively. \mathbf{n} is a unit vector normal to the fluid–structure interface. On the one hand, the fluid and solid stresses in the normal direction on the interface should be equal shown in Equation (8). This condition does not need identical and matching meshes for the fluid and structure domains, but by a way of mapping to map the fluid stress onto the structure nodes.

$$\mathbf{F} = \int (\mathbf{H}^s)^T \underline{\tau}_f ds \quad (9)$$

The $(\mathbf{H}^s)^T$ is the structural element interpolation matrix evaluated at the interface, and \mathbf{F} is the solid nodal force. On the other hand, the displacement of fluid nodes on the coupling interface is enforced by the solid displacement by the use of displacement interpolations of the structure, the fluid displacements are expressed in terms of the structural displacement. A more complete study of the FSI method used in this paper is presented in [27].

2.4. Computational domain and discretisation

The fluid domain is built in the ADINA CFD (ADINA R&D Inc), and the computational domain is presented in Figure 2. All the sizes are normalised by the length of the fish body which is represented by LB. The detailed length is shown in Table 1. The fish model is placed at the middle line of the domain in z -direction. The total length and width of the domain is 11 times and 8 times the length of LB, which is large enough to avoid the boundary effect. Totally, 66,468 triangular elements are used to discretise the fluid domain, and finer mesh is applied around the fish surface to effectively capture the vortex structure without leading to a too much computation cost.

The structure domain is built in ADINA structures, it only consist of three parts as shown in Figure 1; their dimensions are the same with those described in fluid

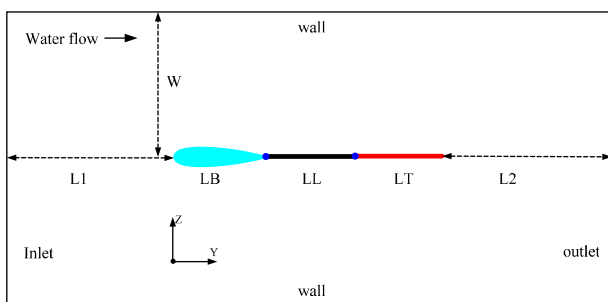


Figure 2. Fluid computational domain for the present study.

domain in Table 1. The fish body is discretised by triangular elements while the caudal fin is discretised by beam elements. Totally, 1061 triangular elements and 150 beam elements are used.

The grid independency is confirmed by checking different number of the grids. We double the grid numbers of the solid domain and fluid domain, the R–R case (described in Section 3) is used in the test. Same condition is carried out, for example, the kinematic frequency is 1 HZ. As shown in Figure 3, the maximum difference in the thrust force and lift force is 3.6 and 0.5%, respectively, indicating that the original mesh resolution is acceptable.

2.5. Simulation condition

The fluid domain and structure domain are solved in ADINA FSI together. Direct coupling is adopted which is a strong interaction between structure and fluid compared with iterative couple since it solves the fluid equations and structure equations in one equation set of every step. In the fluid domain, the fluid is modelled as incompressible water with a density of 1000 kg/m^3 and viscosity of 0.001 Ns/m^2 . Transient analysis is adopted. The boundary conditions include: inlet, outlet, wall and FSI interface. A velocity is applied in the inlet boundary and no-slip wall condition is applied for the upper and lower boundaries. The whole fish model is set as the FSI interface boundaries. In the structure domain, the structure is defined as linear isotropic, elastic material with various parameters listed in the latter section. Implicit schemes are used. The time step is $\Delta t = 0.0025 \text{ s}$, totally 10 s is investigated in our simulation. Meanwhile, the harmonic motion is applied as a linear ramp function for the first 1 s to reach the full load in order for an easier convergence. The fin model performs large motions in the fluid, so adaptive mesh is employed in the fluid domain for mesh regeneration.

3. Results

In this section, computational results are presented and discussed. To investigate the hydrodynamic forces of the two-links caudal fin, several cases are firstly presented as shown in Table 2.

The computation models are divided into two groups – consistent flexibility and variable flexibility. In the consistent flexibility group, the leading link and tailing link share the same flexibility. Three cases are studied, R-R case represents both the two links are rigid and share a large Young's modulus, M-M cases represents the two links are medium flexible, and F-F cases represents the two links are flexible and possess a small Young's modulus. For the variable flexibility group, two cases are modelled. R-F case means the leading link is rigid while the tailing link is flexible. The F-R case is the opposite.

Table 1. Parameter values of the computation domain.

Parameter	Non-dimensional specifications	Description
L1	3	Distance of the leading link and inlet
LB	1	Length of the fish body
LL	1	Length of the leading link
LT	1	Length of the tailing link
L2	5	Distance of the tailing link and outlet
W	4	Distance of the fish model and the computational upper edge

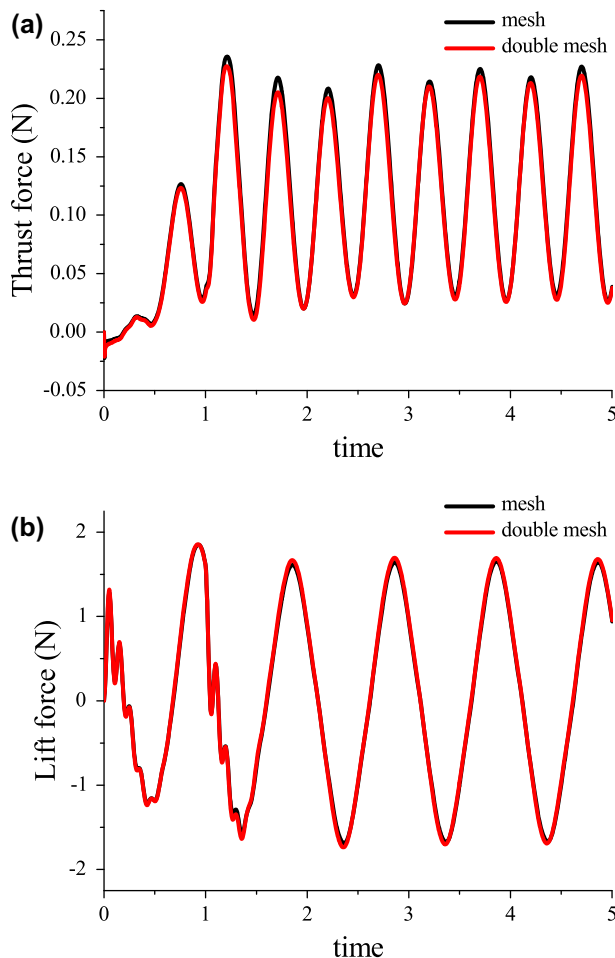


Figure 3. Time history of the thrust and lift forces of two different grid resolutions: (a) thrust force, (b) lift force.

Table 2. Flexibility of the links.

		Leading link	Tailing link
Consistent flexibility	R-R case	Y: 2 GPa	Y: 2 GPa
	M-M case	Y: 20 MPa	Y: 20 MPa
	F-F case	Y: 0.2 MPa	Y: 0.2 MPa
Variable flexibility	R-F case	Y: 2 GPa	Y: 0.2 MPa
	F-R case	Y: 0.2 MPa	Y: 2 GPa

Note: Y means the Young's modulus.

3.1. Effect of fin flexibility

We first conduct simulations to investigate the hydrodynamic performance of the link flexibility. The sinusoidal pitching motion is applied on the leading link. All the five cases share the same kinematic parameters. The pitching frequency is 1 Hz, the pitching amplitude is 0.1, the hinge stiffness is 0.1 Nm/rad, the speed of water flow is 0.01 m/s and the Reynolds number is 2250.

The thrust force and lift force are shown in Figure 4. The thrust force is along the fish body direction, namely the Y component of the fluid force acting on fish shown in Figure 2, while the lift force is perpendicular to the fish body, namely the Z component. It is seen that the frequency of all the thrust force doubles the frequency of driven motion, while the lift force shares the same frequency with the driven motion. In Figure 4(a), the time history of thrust force is shown, it is found that obvious thrust force in the whole cycle is generated for the R-R, M-M and R-F cases. The R-R case generates thrust force with a peak of 0.23 N, while the M-M case with a smaller peak of 0.14 N. The R-F case performs the best, which exhibits the largest peaks about 0.42 N and larger mean thrust force. For the rest two cases, the magnitude of thrust force is very small compared with the previous three cases. For F-F case, it can primarily generate thrust force with slight drag force in a cycle. And for case F-R, it can barely generate thrust force and the force amplitude is the smallest. Moreover, it is seen that the forces show an apparent phase difference, their peaks arrive at different time sequence, which may result from the flexible structure delay response. In Figure 4(b), the lift force is mainly symmetrical around zero for all cases, since we conduct a symmetrical motion. The R-F case generates the largest peaks, and the R-R and M-M cases nearly share the same peaks, while the peaks of the other two cases are relatively smaller.

The pressure contours of two chosen cases are compared at specified time sequences shown in Figure 5. All of the data are obtained from 4 s to 5 s. For the R-R case, it just sheds a tailing edge vortex (TEV) at $t/T = 0$, then when it moves on to $1/8 T$, high- and low-pressure centres occur along the fin; at this time, the leading link moves up clockwise, driving the tailing link up;

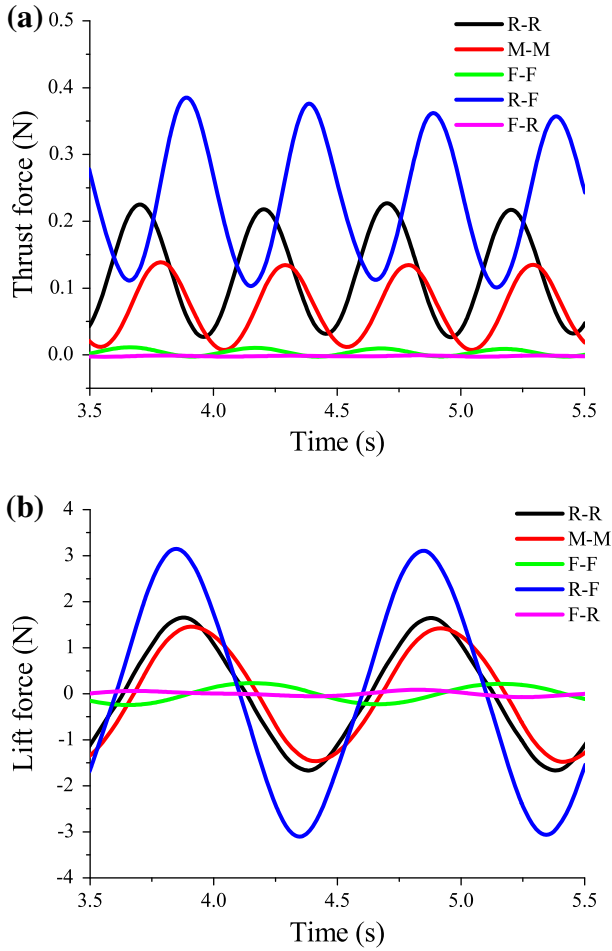


Figure 4. Time history of the thrust and lift forces for five cases.

however, the tailing link rotates passively and moves anticlockwise. At $t/T = 1/4$, the leading link reaches the maximum pitching angle, but the tailing link inclines with certain angle, due to delayed rotation. The leading link generates low-pressure centre above the link and high-pressure centre below, which is the opposite for the tailing link. At $3/8 T$, the high- and low-pressure centres grow stronger and then at $1/2 T$, the TEV sheds from the fin tip. For the next half cycle, the fin pitches downstroke and performs an opposite process. For the R-F case, the caudal fin deforms greatly and the pressure contours differs much. At $0 T$, the TEV is still attached on the fin tip and the tailing link shows downward deformations. High-pressure centre occurs along the upper side of both links while low-pressure centre occurs below the links. Time goes on to $1/8 T$, the TEV sheds from the fin tip and the tailing link nearly recovers to the straight shape which means it undergoes relatively small hydrodynamic force. Then for $1/4 T$, it is seen that the leading link reaches the maximum pitching angle,

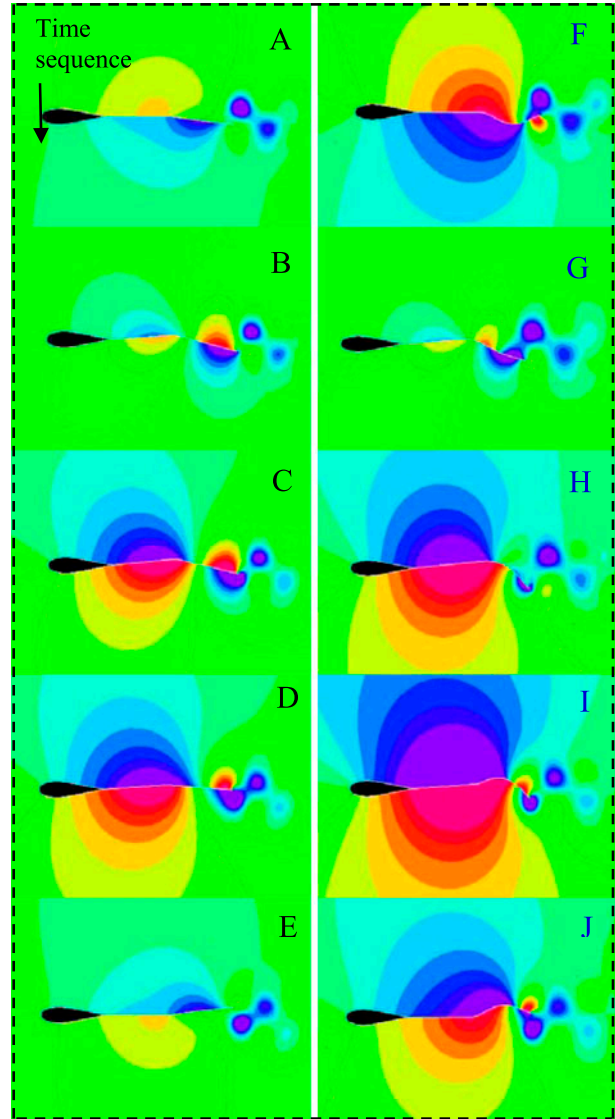


Figure 5. Pressure contours of the fluid field for R-R case (left column) and R-F case (right column). Contours range from -5 to 5 . The time sequences are $0 T$, $1/8 T$, $1/4 T$, $3/8 T$ and $1/2 T$.

and the tailing link deforms greatly under the hydrodynamic force. Compared with the same time sequence of the R-R case, it is found that no high-pressure centres occur above the tailing link. At $3/8 T$, the pressure contours of two cases are similar, but it is seen that the pressure is stronger in R-F case and the high-pressure centre has spread from the leading link to tailing link to a large degree. Then at $1/2 T$, the second TEV is also attached with the tailing link, which lags than R-R case. The pressure contours are also stronger than that of the R-R case.

The typical variations of instantaneous thrust force with instantaneous lift force of the five cases are shown in Figure 6, in which the direction, profile and

magnitude of the fin hydrodynamic force are more clearly presented. The corresponding time history plot is shown in Figure 4. It is seen that all the force plots seem like insect wing, while the force of R-R case shows a positive shape with the other cases showing upside-down shapes. The force of R-F case possesses the largest thrust and lifts peaks, while the force for R-R and M-M cases is more compact with lower thrust force and smaller lift force. For F-F and F-R cases, both the thrust and lift force are much smaller, which seems a bad option for the structure design of the caudal fin, the detailed mean thrust force and lift peaks are presented in latter section.

The R-R and R-F cases are labeled by letters which coincide with Figure 5, which indicates the time course of the force variation. For the same moment in a cycle, it is noticed that the force start point differs much and undergoes different trajectories which result from the flexibility response of the structure. At 0 T, the transient force point A is at lower location of the inner edge of the wing for R-R case suggesting a lower thrust force with medium lift force, while the point F is at the middle location of the inner edge of the upside-down wing for R-F case indicating a relatively large thrust force with medium lift force. Then At 1/8 T, it is seen that the R-R case almost generates no lift force with relatively large thrust force while the R-F case produces the lowest thrust force with relatively small lift force at this second. As time goes on, the thrust force in R-F case increases to the peaks while the lift force decreases to the lowest point at 3/8 T; the lift force also decreases for R-R case, but the thrust force increases first and then decreases. When time arrives at 1/2 T, both of their lift force increase, while the thrust force of R-F case decreases much with the thrust force of R-R crosses the lowest point. For the next half cycle, the forces move along the

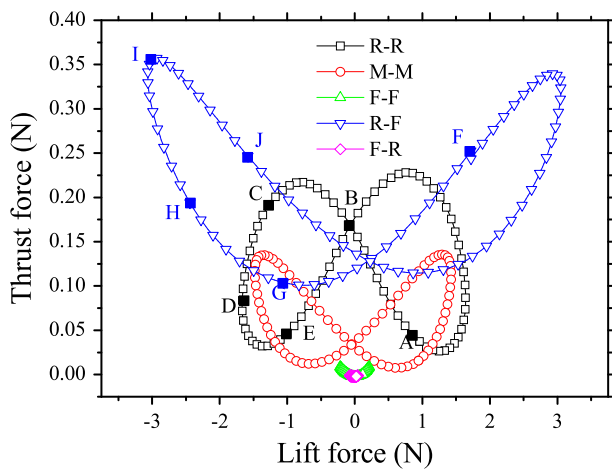


Figure 6. Instantaneous thrust force with lift force plot for five cases.

other half of the wing. It is found out that the forces undergo the opposite developing processes as the letters indicated in the plot, namely, the twine direction of ∞ is opposite.

The pressure contours of the other three cases are presented in Figure 7. For the M-M case, it can also shed two TEVs in a cycle, but its strength of the pressure centres is lower than that of the R-R case. While for the other two cases: F-F and F-R case, it can be seen that the total caudal fin undergoes deformations. It moves like the wave spreading and several high- and low-pressure centres attached along with the fin. However, it is seen that their pressure contours are much weaker than the other cases, which suggests less displacement and disturbance to the fluid field leading to less force generation, and this is verified in Figure 4. In the two cases, the F-R case produces the weakest pressure contour which is caused by the flexibility of the tailing link. Since its tailing link is rigid, it owns large inertial force and would not deform, and it decreases the displacement and deformation of the leading link in return.

The structure displacement and deformation are also illustrated. The hinge and fin tip are investigated as shown in Figure 8. The Z-direction displacement of the hinge reflects the leading link's displacement and deformation, while the displacement of the fin tip is a comprehensive index for the whole caudal fin. In Figure 8(a), it is seen that, for the R-R and R-F cases, the Z-displacements coincide with each other, because the rigid leading link is adopted in the both cases. The rigid link carries with no deformation and responds immediately with no-phase delay. In the M-M case, the magnitude of the displacement is smaller and a slight phase difference occurs. For the F-F and F-R cases, the phase difference is apparent and the leading link produces smaller z-displacement. For the fin tip displacement, R-F case exhibits the largest peaks which owe to the large displacement of the leading link and large deformation of the tailing link as show in Figure 5. The M-M and R-R cases show similar peaks. And the F-R case follows with the F-F case presenting the smallest fin tip displacement.

3.2. Effect of the pitching frequency

A series of numerical experiments are conducted to investigate the effect of the pitching frequency. The hydrodynamic forces are presented in Figure 9.

For the consistent flexibility group, it is seen that the R-R case produces larger thrust force than other cases for a low frequency of 0.5 Hz. It generates 0.12 N average thrust force. When the frequency increases, the mean thrust force increases as expected. When the frequency increases from 1 to 1.5 Hz, the mean thrust force

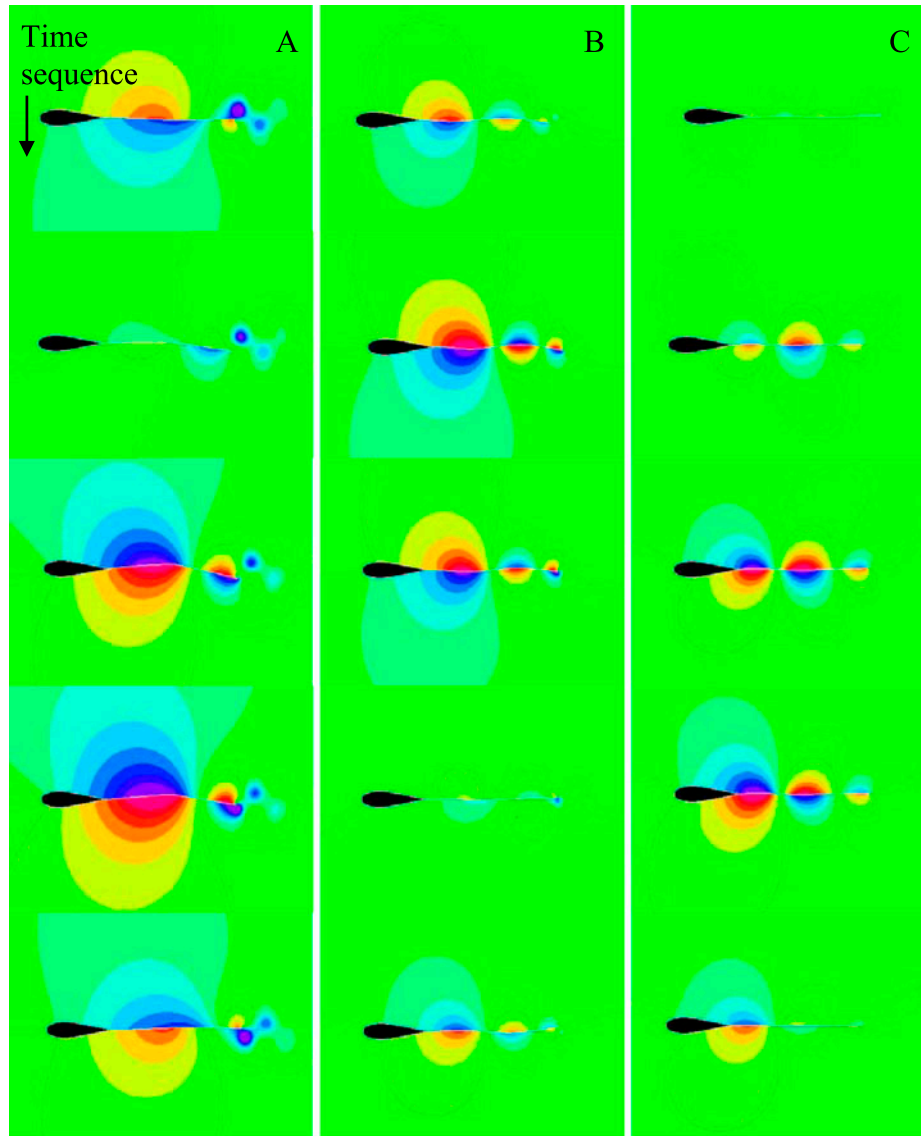


Figure 7. Pressure contours for the other three cases. Column A: M-M case, contours range from -5 to 5 ; column B: F-F case, contours range from -1.5 to 1.5 ; column C: F-R case, contours range from -0.5 to 0.5 . The time sequences are defined in Figure 5.

increases by 20%. With the same increase in frequency from 1.5 to 2 Hz, the force increases by 38%. It indicates that the thrust force increases with a higher rate at higher frequency for the R-R case. This trend fits the M-M case for lower frequency too. When the frequency is below 1.5 Hz, its mean thrust force is smaller than R-R case, but at 1.5 Hz, its magnitude is 0.33 N which is 2.2 times that of R-R case. When the frequency is higher than 1.5 Hz, the M-M case shows a great decay in the force. The result suggests the M-M caudal fin possesses a positive coupling with 1.5 Hz or even resonates around this frequency which leads to a peak in the performance. This phenomenon indicates that there is an optimal-driven frequency for specified fin model to achieve the best performance. These finds conform to

the previous studies.[19,29,30] For the case F-F, the mean thrust force and lift force peaks are much smaller than the other cases for all frequency. It can nearly generate no thrust force in a cycle. One reasonable explanation is that since in this case, the caudal fin is very flexible, the motion is applied on the leading link and it spreads to the fin tip like the waves, the whole fin oscillates. The displacement fin is small (in Figure 8), and the pressure contours are weaker (in Figure 7) resulting in its small thrust and lift force. For the variable flexibility group, the R-F presents an impressive performance. The thrust increases with the frequency greatly, but the rate slows down, from 0.5 to 1 Hz, it increases by 639%; while for the other, same frequency amount increase, it only increases by 73 and 23%. The mean

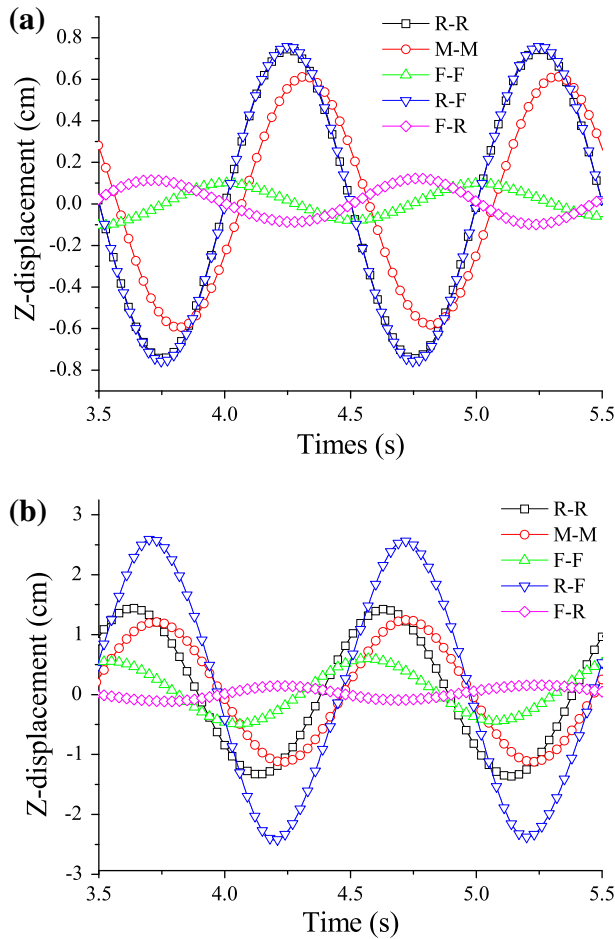


Figure 8. Z-displacement of the hinge (a) and the fin tip (b).

thrust force exceeds the R-R case at 1 Hz, and behaves best for the rest. For the F-R case, its performance is as bad as the F-F case, since the leading link is too flexible; the whole caudal fin can no longer generate enough amplitude and the mean thrust force is very small.

The mean lift force is not suitable in our case since it mainly equals zero, so the peak of the lift force is analysed. It is seen that the lift peaks show similar trend with the corresponding thrust force in each case, but amplitudes and ratio differ. For example, for the R-R case, the increase ratio of lift force is larger at higher frequency and its magnitude ranks first for 2 Hz. For the M-M case, the lift force peak also first increases with frequency and then decreases, it reaches the largest value at 1.5 Hz and the value is larger than the other cases.

3.3. Effect of the hinge stiffness

For a two-links caudal fin, the stiffness of the hinge accounts much, and it will affect the response of the tailing link. One extreme limit is that the stiffness is infinite,

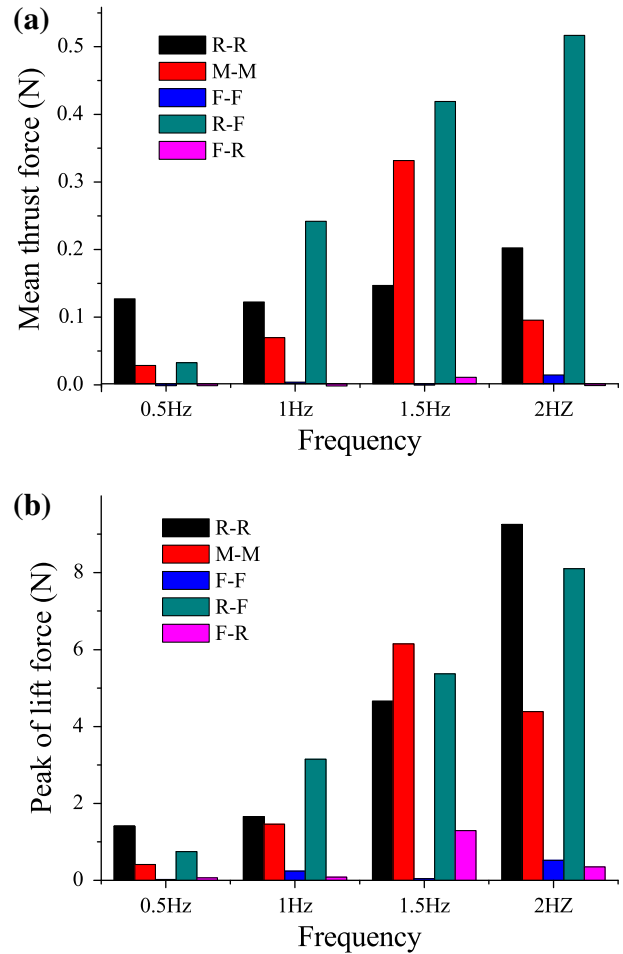


Figure 9. Mean thrust force (a), peaks of the lift force (b) for five cases with different pitching frequency. Means are based on five consecutive periods.

the two links will act as one link, while for the contrary condition, the stiffness is zero, and the tailing link will rotate freely under the fluid force and inertial force. In this section, we vary the hinge stiffness and investigate its coupling effect with the link flexibility. The pitching frequency is 1 Hz, and the pitching amplitude is 0.1.

When the hinge stiffness decreases to 0.01 Nm/rad, the structure response possesses striking difference as shown in Figure 10. It is seen that the M-M case produces the largest z-displacement at the hinge point which is 312% that of the R-R and R-F case. Meanwhile, compared with the displacement in Figure 8(a), it increases by 277% in the peak magnitude. The time delay or the phase difference is more obviously. At the fin tip, its displacement also increases much. Its pressure contours are shown in Figure 11. It is seen that the leading link bends to a large degree and the tailing link rotates largely which differs with the Figure 7. It also sheds strong TEVs from the fin tip. For the others cases, the structure

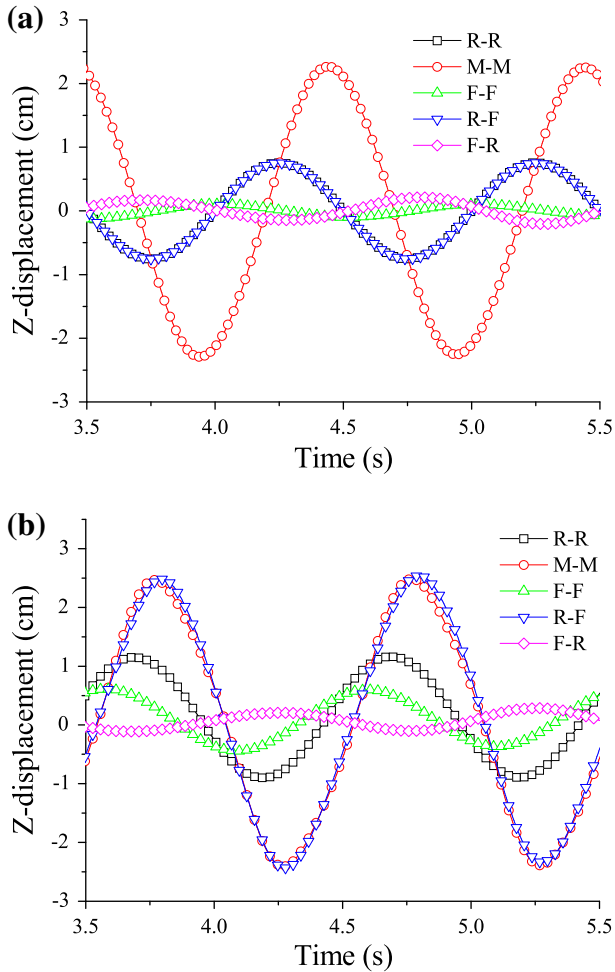


Figure 10. Z-displacement of the hinge (a) and the fin tip (b).

displacement variations are not prominent. The corresponding thrust and lift plot is shown in Figure 12, it is seen that the M-M case generates much larger thrust force and lift force peaks than the other cases, and its shape curve sinks to a narrow. However, it is noticed that it will produce drag force for sometime in a cycle which is different with that of Figure 6. The detailed mean thrust force and lift force peaks are presented in Figure 13.

In the consistent flexibility group, the mean thrust force for the R-R case possesses a positive relationship with the stiffness of hinge. The average thrust force decreases by 264 and 351% as the hinge stiffness decreases, respectively. The M-M case demonstrates a striking different trend. When the spring stiffness decreases, the mean thrust force increases. From 0.1 Nm/rad to 0.01 Nm/rad, the force increases by 515% with 0.43 N and from 0.01 Nm/rad to 0.001 Nm/rad, it increases by 12% with 0.48 N. It shows dominant leading role compared with other cases when the hinge stiffness is small. For the variable flexibility group, the R-F

case exhibits similar trends with the R-R case, but its magnitude is much larger. For hinge stiffness of 0.1 Nm/rad, the R-F case behaves better with 0.24 N. For the lift peaks, the R-R case increases with the decrease in stiffness which is different with the trend of mean thrust force. The M-M case also generates larger peaks with stiffness of 0.01 Nm/rad and 0.001 Nm. For the F-F case, the lift peaks varies little, while for F-R case, the lift force increases much.

4. Discussion

The fish fins undergo great deformations when they swim, which is an interaction of the solid structure and the fluid field. The flexible structure plays an important role in the force generation. However, the distribution of flexibility is anisotropic because of the complicated structure of the fins. By direct observation and measurement, it is found that the fish fin is harder at the base and more flexible at the fin tip.[31] In this regard, we develop a two-dimensional model in the present study in which the chord-wise flexibility is considered. The caudal fin consists of two flexible links. Two comparisons are conducted. On the one hand, we uniform the flexibility of the two links from rigid to flexible. We study flexibility's effect on the hydrodynamic performance combining with the hinge stiffness. On the other hand, two more variable flexibility caudal fins are modelled. One is harder at the base and softer at the tip, while the other one is the opposite.

It is seen from the results that flexibility is not a guarantee for a better propulsion performance and its performance is closely connected with the frequency. For the frequency tested in this work, the R-R case can generate more thrust force than other cases when the frequency is low. However, when frequency increases, flexible fins show advantages. The R-F and M-M cases can both generate more thrust force, of which the M-M case peaks at particular driven frequency with previous research that implies optimal frequency exists for flexible fins.[20,29,30] The R-F case which mimics the variable flexibility fin seems a good choice for the caudal fin design, as it can generate relatively large thrust force when frequency is higher as shown in Figure 9. However, it is also found that its increasing rate slows down when the frequency increase, which means the force will level off or decay at a higher frequency. When the fin is too compliant, its performance is poorer than other cases; it generates less thrust force and lift force nearly for all frequencies as shown for F-F case and F-R case, the results are consistent with that of [20]. One reasonable explanation is that the leading link is too flexible, it oscillates and the motion spreads like waves which cannot efficiently interact with the water and produce thrust force. Besides, it is seen that large lift force peak comes

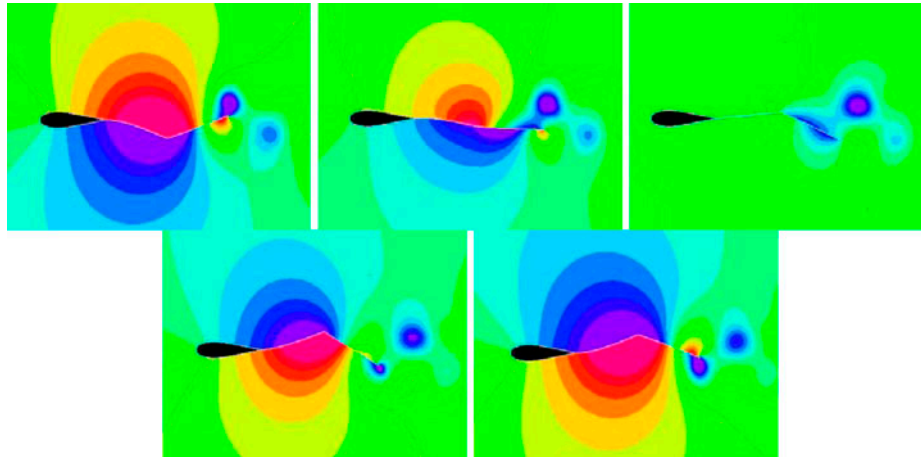


Figure 11. Pressure contours of M-M case. Contours range from -15 to 15 . The time sequences are defined in Figure 5.

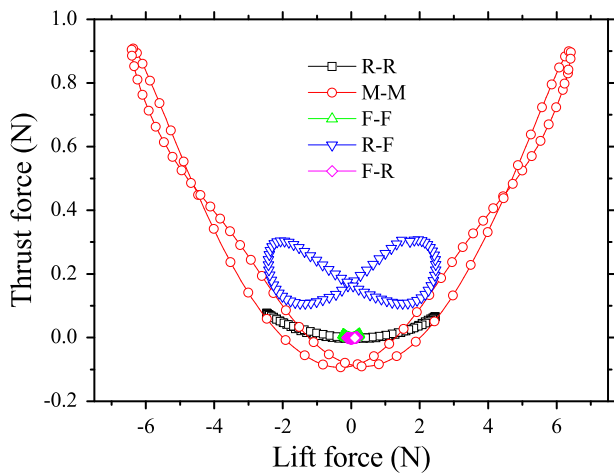


Figure 12. Instantaneous thrust vs. lift plot for hinge stiffness of 0.01 Nm/rad. The pitching frequency is 1 Hz.

along with large mean thrust force. The mean thrust force is beneficial for fish swimming, while the lift force is hard to decide. The lift force can balance the fish weight, but too large lift peak will result in the instability of fish body and lead to oscillate ups and downs, which may be a disadvantage. To reduce the lift force, one design is to use two parallel fins which moves in an opposite phase. In this way, the thrust force may be enhanced while the lift force may be counteracted.

For the response of the caudal fin, a phase-difference response should be noticed, as shown in Figures (4, 8 and 10), both in the force and displacement. For example, in Figure 8, it is seen that the displacement of hinge of R-R and R-F cases are the same and shows no-phase delay with the driven motion because the leading links are rigid; but for M-M case, a slight phase lag is seen and for the F-F and F-R cases, the phase lag is apparent,

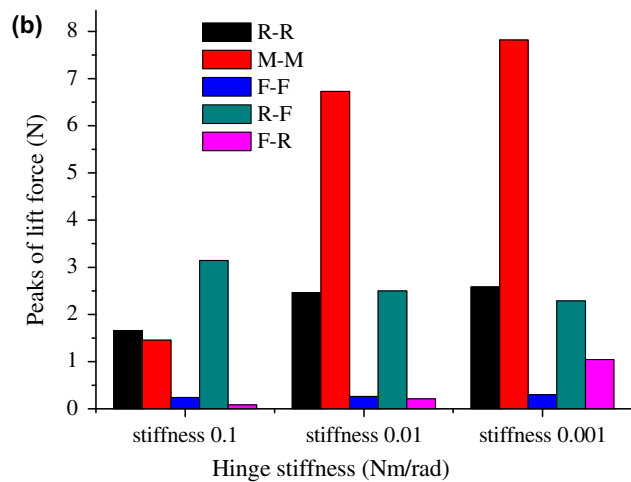
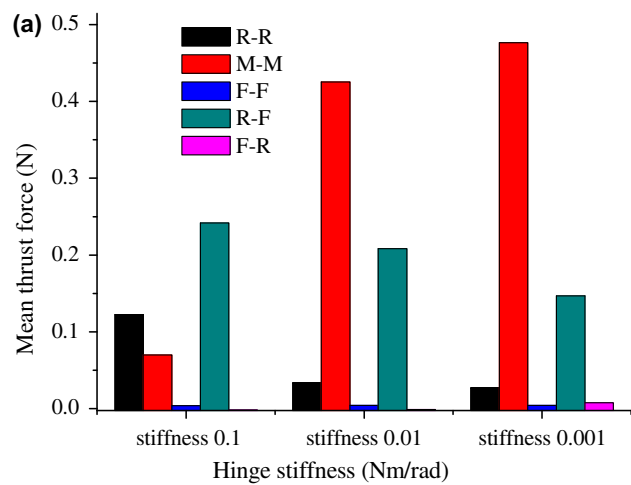


Figure 13. Mean thrust force (a), peak of the lift force (b) for five cases with different hinge stiffness.

the results agree with that of [13]. The phase lag comes from the structure response to the driven motion and fluid force, and will influence the hydrodynamic forces. Park et al. come up with a half- π phase-delay condition to maximum the thrust force under zero-velocity condition,[32] but it is much more complicated for a swimming fish with hinged fins. Meanwhile, the time delay reminds researchers to carefully choose flexible material for multiple flexible fin design, since the fins need to cooperate with each other, the time delay should be considered to produce an integral positive effect.

The hinge stiffness is of big importance as it is a vital part of the total fin flexibility. It affects the motion spread from the leading link to tailing link and the reaction force from the tailing link to the leading link. The larger the hinge stiffness, the stronger coupling between the two links. Nakabayashi et al. conducted experiments by changing the effective length of spring to change the stiffness of two connected plates.[15] They discovered that the swimming speed possesses a complex relationship with the effective stiffness. In our simulation experiments, we fix the swimming speed and measure the average thrust force. For the R-R case, its mean thrust force decreases with the hinge stiffness in our hinge stiffness range as shown in Figure 13. However, when the flexibility of links is coupled, the results show difference. It is seen that for the R-F cases, the mean thrust force decreases with the hinge stiffness, but for the M-M case, the mean thrust force shows an abnormal increase up to 515% from hinge stiffness form 0.1 Nm/rad to 0.01 Nm/rad. Then when the stiffness is too low, the increasing rate slows down. It also shows an opposite trend for the thrust force and lift force in R-R case; the results show a more complicated coupling between the hinge stiffness and the flexibility of the links.

5. Conclusions

In the present work, the hydrodynamic performance of a two-dimensional simplified fish model with a flexible articulated caudal fin is investigated. The caudal fin is composed of two links which are connected by a hinge. The flexibility of the caudal fin is determined by the flexibility of the links and hinge stiffness. Various flexibility fins are studied through a coupled fluid-structure interactions scheme.

The results demonstrate that the flexibility is not always beneficial for the hydrodynamic force. At a low frequency, the rigid-rigid caudal fin produces larger thrust force than other cases, while the rigid-flexible and medium-medium fins perform better with a higher frequency. And nearly for all the frequencies considered, the flexible-flexible and flexible-rigid fins perform

poorly. Furthermore, an optimal frequency exists for the flexible structure to achieve the best performance. Besides, the rigid-flexible fin shows a better performance than other cases with larger hinge stiffness. But when the hinge stiffness decreases, the medium-medium case presents an interesting performance. Its mean thrust force increases with the decreasing of the hinge stiffness which is different with other cases. The results will be useful for the flexible underwater propulsion, and the multi-flexible-links fin can guide the design of flexible propeller.

Supplementary material

The supplementary material for this paper is available online at <http://dx.doi.org/10.1080/01691864.2014.957722>

Funding

This work is supported by National Natural Science Foundation of China (50975270 51375468) and the Fundamental Research Funds for the Central Universities of China (WK2090090002).

Notes on contributors



Bo Liu was born in NanChong, SiChuan, China, in 1988. He received the Bachelor's degree of Engineering in Mechanical Engineering in 2010 from University of Science and Technology of China. He is currently studying for PhD degree now. His interest is focused in the pectoral fin design and numerical simulation, including computational fluid dynamics and fluid-structure interactions.



Shiwu Zhang received the BS degree in mechanical and electrical engineering and the PhD degree in precision instrumentation and precision machinery from the University of Science and Technology of China (USTC), Hefei, China. He is currently an Associate Professor in the Department of Precision Machinery and Precision Instrumentation, USTC. He has also been a Postdoctoral Research Fellow in the Department of Computer Science, Hong Kong Baptist University, Hong Kong. He has led a number of research programs sponsored by the National Science Foundation of China, Chinese Academy of Sciences, Chinese State High-Tech Development Plan, Chinese Aeronautical Foundation, etc. He has authored or coauthored more than 50 technical peer-reviewed papers. His current research interests include smart materials and their applications in bioinspired robots, amphibious robots, and terradynamics that involves interactions between locomotion mechanisms and sandy or muddy substrates.



Fenghua Qin received his Bachelor and PhD degrees in mechanical engineering from University of Science and Technology of China in 1999 and 2005, respectively. He is currently an associate professor with Department of Modern Mechanics, University of Science and Technology of China. His research interests are biomimetic robots and microfluidic.



Jie Yang received the Graduate degree from the Department of Physical Chemistry, Beijing University of Science and Technology, Beijing, China, in 1969. He is currently a Professor in the Department of Precision Machinery and Precision Instrumentation, University of Science and Technology of China, Hefei, China. He leads several research groups focusing on intelligent robots supported by the National

Science Foundation of China and the 863 Project. His research interests include intelligent robots, precision machinery materials, and high-speed photography.

References

- [1] Chopra MG, Kambe T. Hydrodynamics of lunate-tail swimming propulsion. Part II. *J. Fluid. Mech.* 1977;79:49–69.
- [2] Katz J, Weihs D. Hydrodynamic propulsion by large amplitude oscillation of an airfoil with chordwise flexibility. *J. Fluid. Mech.* 1978;88:485–497.
- [3] Liu P, Bose N. Propulsive performance of three naturally occurring oscillating propeller planforms. *IEEE J. Ocean Eng.* 1993;20:57–75.
- [4] Nauen JC, Lauder GV. Hydrodynamics of caudal fin locomotion by chub mackerel, *Scomber japonicus* (Scombridae). *J. Exp. Biol.* 2002;205:1709–1724.
- [5] Lauder GV. Function of caudal fin during locomotion in fishes: kinematics, flow visualization, and evaluational patterns. *Am. Zool.* 2000;40:101–122.
- [6] Liao B, Li Z, Du R. Robot fish with a novel biomimetic wire-driven flapping propulsor. *Adv. Robot.* 2014;28:339–349.
- [7] Yu J, Wei C. Towards development of a slider-crank centered self-propelled dolphin robot. *Adv. Robot.* 2013;27:971–977.
- [8] Marchese AD, Onal CD, Rus D. Autonomous soft robotic fish capable of escape maneuvers using fluidic elastomer actuators. *Soft Robot.* 2014;1:75–87.
- [9] Ziegler M, Lida F, Pfeifer R. “Cheap” underwater locomotion: roles of morphological properties and behavioural diversity. *Proceedings of Climbing and Walking Robots*; 2006.
- [10] Heathcote S, Wang Z, Gursul I. Effect of spanwise flexibility on flapping wing propulsion. *J. Fluid Struct.* 2008;24:183–199.
- [11] Bi S, Cai Y. Effect of spanwise flexibility on propulsion performance of a flapping hydrofoil at low Reynolds number. *Chin. J. Mech. Eng.* 2012;25:12–19.
- [12] Tay WB, Lim KB. Numerical analysis of active chordwise flexibility on the performance of non-symmetrical flapping airfoils. *J. Fluid Struct.* 2010;26:74–91.
- [13] Heathcote S, Martin D, Gursul I. Flexible flapping airfoil propulsion at zero freestream velocity. *AIAA J.* 2004;42:2196–2204.
- [14] Ziegler M, Pfeifer R. Sensory feedback of a fish robot with tunable elastic tail fin, biomimetic and biohybrid systems. Berlin Heidelberg: Springer; 2013. p. 335–346.
- [15] Nakabayashi M, Kobayashi R, Kobayashi S, Morikawa H. Bioinspired propulsion mechanism using a fin with a dynamic variable-effective-length spring-evaluation thrust characteristics and flow around a fin in a uniform flow. *J. Biom. Sci. Eng.* 2009;4:82–93.
- [16] Liu B, Xu M, Wang L, Yang J, Zhang S. Fluid-structure interaction study on a flexible robotic pectoral fin. *IEEE International Conference on Mechatronics and Automation*, 2012; Chengdu, China. 2012:220–225.
- [17] Hamamoto M, Ohta Y, Hara K, Hisada T. Application of fluid-structure interaction analysis to flapping flight of insects with deformable wings. *Adv. Robot.* 2007;21:1–21.
- [18] Zhu Q, Shoel K. Propulsion performance of a skeleton-strengthened fin. *J. Exp. Biol.* 2008;211:2087–2100.
- [19] Zhu Q. Numerical simulation of a flapping foil with chordwise or spanwise flexibility. *AIAA J.* 2007;45:2448–2457.
- [20] Esposito CJ, Tangorra JL, Flammang BE, Lauder GV. A robotic fish caudal fin: effects of stiffness and motor program on locomotor performance. *J. Exp. Biol.* 2012;215:56–67.
- [21] Eldredge JD. Numerical simulation of the fluid dynamics of 2D rigid body motion with the vortex particle method. *J. Comput. Phys.* 2007;221:626–648.
- [22] Eldredge JD. Dynamically coupled fluid-body interactions in vorticity-based numerical simulations. *J. Comput. Phys.* 2008;227:9170–9194.
- [23] Toomey J, Eldredge JD. Numerical and experimental study of the fluid dynamics of a flapping wing with low order flexibility. *Phys. Fluids.* 2008;20:073603.
- [24] Wan H, Dong H, Huang G. Computational fluid-body interaction of hinge connected flapping Plate in Hover. 49th AIAA Aerospace Sciences Meeting. 2011;379:2011.
- [25] Le TQ, Ko JH, Byun D, Park SH, Park HC. Effect of chord flexure on aerodynamic performance of a flapping wing. *J. Bion. Eng.* 2010;7:87–94.
- [26] Tang J, Viieru D, Shyy W. A study of aerodynamics of low Reynolds number flexible airfoils. *AIAA Paper.* 2014:2007–4212.
- [27] Rugonyi S, Bathe kJ. On finite element analysis of fluid flows fully coupled with structural interactions. *Comp. Modeling Eng. Sci.* 2001;2:195–212.
- [28] Scotti CM, Finol EA. Compliant biomechanics of abdominal aortic aneurysms: a fluid-structure interaction study. *Compu. Struct.* 2007;85:1097–1113.
- [29] Lauder GV, Madden PGA, Tangorra JL, Anderson E, Baker TV. Bioinspiration from fish for smart material design and function. *Smart Mater. Struct.* 2011;20:094014.
- [30] Akhta I, Mittal R, Lauder GV, Drucker E. Hydrodynamics of a biologically inspired tandem flapping foil configuration. *Theor. Comp. Fluid Dyn.* 2007;21:155–170.
- [31] Yan Q, Wang L, Liu B, Yang J, Zhang S. A novel implementation of a flexible robotic fin actuated by shape memory alloy. *J. Bion. Eng.* 2012;9:156–165.
- [32] Park YJ, Jeong U, Lee J, Kwon SR, Kim HY, Cho kJ. Kinematic condition for maximizing the thrust of a robotic fish using a compliant caudal fin. *IEEE Trans. Robot.* 2012;28:1216–1227.